batteries

MDPI

Article

Rapid State of Health Estimation Strategy for Retired Batteries Based on Resting Voltage Curves

Haihong Huang [1], Xin Liu [1,*], Wenjing Chang [2] and Yuhang Wang [3]

[1] School of Electrical Engineering and Automation, Hefei University of Technology, Hefei 230009, China; hhh@hfut.edu.cn
[2] State Grid Anhui Ultra High Voltage Company, No. 397, Tongcheng South Road, Baohe District, Hefei 230000, China
[3] State Grid Anhui Electric Power Research Institute, No. 299, Ziyun Road, Hefei 230000, China; 2019110381@mail.hfut.edu.cn
* Correspondence: hfutlx@hotmail.com

Abstract: Retired batteries are approaching the recycling peak, and their secondary utilization can prevent resource waste and environmental pollution from battery retirement. Evaluating the state of health (SOH) of retired batteries is crucial for secondary use. However, estimating the SOH of retired batteries is time-consuming and energy-intensive. To address the problem, this paper proposes a rapid estimation strategy based on resting voltage curves. After discharging retired batteries to the same voltage, variations in the remaining state of charge (SOC) exist among batteries with different SOHs. These SOC differences lead to distinct trends in the resting voltage curves for varying SOH batteries. Our approach analyzes health features from these resting voltage discrepancies, ultimately achieving a fast estimation of retired batteries' SOH. Additionally, during the data collection of datasets, some batteries may form outliers due to measurement errors. This paper analyzes the impact of outlier quantity on the accuracy of regression models for SOH estimation and proposes using the DBSCAN clustering algorithm to identify and mitigate the influence of outliers, eventually enhancing the precision of SOH estimation.

Keywords: lithium iron phosphate battery; static voltage; state of health; fast estimation

Academic Editor: Pascal Venet

Received: 15 December 2024
Revised: 28 January 2025
Accepted: 5 February 2025
Published: 8 February 2025

Citation: Huang, H.; Liu, X.; Chang, W.; Wang, Y. Rapid State of Health Estimation Strategy for Retired Batteries Based on Resting Voltage Curves. *Batteries* **2025**, *11*, 66. https://doi.org/10.3390/batteries11020066

1. Introduction

In recent years, the new energy industry has experienced rapid development. Lithium-ion batteries, due to their high energy density, low cost, and long lifespan, have found applications in electric vehicles, energy storage, and other fields. Over time, an increasing number of traction batteries face the challenge of retirement and the subsequent question of how to handle them. Typically, when the remaining state of health (SOH) of a battery drops to the range of 70% to 80%, it is considered suitable for retirement and recycling. However, issues such as energy storage system failures, vehicle malfunctions, and partial module-level battery faults can lead to the retirement of all batteries within a module, resulting in varying performance parameters among retired batteries [1–3]. Reusing well-performing retired batteries can significantly conserve resources and prevent environmental pollution.

SOH serves as a critical factor in determining the feasibility of secondary utilization scenarios for retired batteries. It describes the aging level of a retired battery. As SOH decreases, both battery range and safety gradually diminish. Therefore, research on estimating SOH for retired batteries is significantly important [4]. Since SOH cannot be directly measured, its estimation relies on observed battery voltage, current, and temperature data. However, studies on SOH assessment for retired batteries remain relatively scarce, with

existing research primarily focused on online scenarios [5,6]. The ampere-hour integration method, which accumulates the charge released by a battery during discharge, is commonly used for SOH estimation. While this method accurately determines the remaining capacity, it suffers from limitations when applied to long-duration complete charge–discharge cycles, significantly impacting the efficiency of secondary sorting for retired batteries [7]. During vehicle operation, the ampere-hour integration method is affected by current and voltage measurement errors. To enhance online SOH estimation precision, adaptive filtering algorithms, including Kalman filters, particle filters, and neural network algorithms, have been proposed [8–10]. A novel fractional-order model was established, followed by an improved SOH and state of charge (SOC) joint estimation method based on Kalman filtering [11]. Another research study introduced a dynamic migration model combined with particle filtering to estimate battery SOC and SOH jointly [12]. However, these methods are specifically tailored for online scenarios and cannot be directly applied to retired battery sorting without history data [13–15].

Data-driven methods treat batteries as black-box models, analyzing health features (HFs) during the aging process and combining them with artificial intelligence algorithms to estimate SOH. The accuracy of SOH estimation depends on both the choice of artificial intelligence algorithms and the quality of HFs [16]. Commonly, the artificial intelligence algorithms used include artificial neural networks, support vector machines, relevance vector machines, Gaussian process regression, and random forest regression (RFR). Researchers propose novel data-driven SOH estimation based on HFs from battery voltage and temperature data [17]. For instance, particle swarm optimization algorithms have been used to optimize long short-term memory networks for SOH estimation. Additionally, an improved ant colony optimization of a support vector regression (SVR) algorithm was proposed based on history data. Unlike online scenarios, retired battery SOH estimation benefits from abundant computational power and low real-time requirements, making data-driven algorithms suitable for the sorting of retired batteries [18–20]. However, when using datasets containing outliers to estimate battery SOH, the accuracy of SOH estimation can be affected. Outliers may arise due to measurement errors during testing or abnormal operating conditions experienced by batteries. Detecting and handling outliers is crucial to maintaining the accuracy of SOH estimation models [21].

Outlier detection methods generally fall into three categories: statistical models, distance-based methods, and clustering-based methods [22,23]. Statistical models assume that the dataset follows a specific probability distribution, identifying outliers based on their position within this distribution. Distance-based methods calculate distances between data points to determine outliers: points with distances exceeding a threshold are considered outliers. Clustering-based methods group data based on latent features, and outliers often appear as individual points or clusters deviating from the majority of data. However, the form of outliers in HF datasets from retired batteries is not specific, making it challenging to determine precise probability distribution functions or distance thresholds. Therefore, this paper proposes using the DBSCAN clustering method to identify outliers in retired battery datasets, mitigating their impact on training sets.

In addition to artificial intelligence algorithms, HFs significantly impact the accuracy of SOH estimation. Feature extraction is a critical step in assessing SOH for retired batteries, and this process should be both simple and rapid. In online scenarios, HF data from vehicle batteries can be extracted from history data, and the SOC is confirmed, allowing SOH features to be obtained at specific SOC levels. Refs. [5,24] propose extracting HF components from electrochemical impedance spectroscopy (EIS) and then utilizing data-driven algorithms to estimate the SOH of batteries. The acquisition time for EIS generally ranges from a few minutes to a few tens of minutes, making it a rapid method for SOH

estimation. However, EIS varies under different SOCs, which complicates the estimation of SOH for retired power batteries with unknown SOC. Ref. [25] suggests extracting HFs that describe battery SOH from battery operating temperatures, but this approach relies on long-term battery temperature data, which are often unavailable for retired batteries during sorting. Refs. [26,27] investigated battery aging mechanisms through incremental capacity analysis and integrated circuit peak area analysis, combined with regression algorithms to estimate SOH. However, incremental capacity curves depend on complete charge–discharge cycles over extended periods, limiting the application of this method for the rapid sorting of retired power batteries. Ref. [13] proposes a method for estimating battery SOH based on the feature of partial capacity fade extracted from the charging segment, combined with data-driven algorithms. Nevertheless, FPs based on charging curves need to be obtained at specific SOCs for retired batteries, making it difficult to estimate SOH for batteries with unknown SOC. Ref. [28] extracted HFs from relaxation voltage curves and used machine learning methods to build a battery SOH estimation model. Similarly, relaxation voltage curves differ under different SOCs, preventing the estimation of battery SOH using relaxation voltage curves for batteries with unknown SOCs. Ref. [29] studied the relationship between coulombic efficiency and battery capacity fade, noting that batteries with lower coulombic efficiency exhibit faster capacity fade rates and increased SOC inconsistency among batteries. Guo Yongfang et al. proposed a method for predicting battery SOH using short-term voltage recovery, enabling rapid SOH estimation at specific SOCs [30]. Refs. [31,32] propose using OCV curves to estimate battery performance, but obtaining OCV curves requires considerable time. In summary, the acquisition time for relaxation voltage curves or EIS is around several minutes, but they cannot be directly utilized due to the unknown SOC. Obtaining the incremental capacity curves requires charging and discharging the battery with a small current, which can take several hours or even dozens of hours. The ampere-hour integration method takes the longest, requiring more than 2 h. The method proposed in this paper takes, at most, only about 1 h and 3 min, significantly reducing the time required for SOH estimation.

The diverse aging mechanisms result from differences in history environments, discharge depths, and current for assessing retired batteries. The multitude of aging mechanisms results in complex SOH evaluation. Retired batteries exhibit varying SOC levels during testing. Traditional HF acquisition strategies, which rely on SOC, cannot be directly applied. Common methods, such as incremental capacity curves and constant-voltage charging current curves, suffer limitations when estimating SOH for retired batteries. Incremental capacity curves require low-current cycles, and constant-voltage charging involves time-consuming current decay. Therefore, this paper proposes a rapid SOH estimation strategy applicable to retired batteries with diverse and unknown SOCs. This method discharges retired batteries to a specific voltage and extracts HFs from resting curves. Compared to traditional methods, the proposed SOH estimation strategy offers advantages in terms of speed and ease of implementation.

The second section describes the reasons for selecting HFs proposed in this paper from the resting voltage curves and the process of obtaining them. The third section describes the specific process of the rapid SOH estimation method proposed in this paper, as well as how to use the DBSCAN algorithm to filter out outliers in the training dataset. The fourth section verifies the effectiveness of the proposed method by describing the reasons for selecting a discharge voltage of 2.5 V, the impact of outliers on SOH estimation, the improvement in SOH estimation accuracy after removing outliers using the DBSCAN algorithm, and the reduction in SOH estimation time. In summary, this paper makes the following contributions:

(1) The impact of outlier data on the estimation of SOH was analyzed. An anomaly identification method for retired battery data based on the DBSCAN algorithm was proposed, aiming to reduce the influence of outliers on battery data-driven models.

(2) The correlation between the OCV and SOH after discharging lithium iron phosphate batteries to different cutoff voltages was established. Based on this, a rapid SOH estimation method using the OCV curve of retired batteries was proposed, which can significantly reduce the time required for the SOH estimation of retired batteries using low-cost equipment.

2. The Acquisition of Health Features

In this article, SOH refers to the ratio of the current capacity to the capacity of a new battery, reflecting the performance degradation of the battery during long-term use.

$$\mathrm{SOH} = \frac{C_{\mathrm{now}}}{C_{\mathrm{new}}} \tag{1}$$

Selecting HFs highly correlated with SOH can effectively improve the precision of SOH estimation. Feature extraction plays a vital role in assessing the SOH of retired batteries, and HF acquisition strategies should consider both time and equipment costs. Strategies that are low-cost and rapid in HF extraction enhance the efficiency of retired battery reuse. This paper proposes extracting HFs for SOH estimation from the resting voltage, which is described as follows:

Step 1: Discharge the battery at a constant current of 1C to 2.5V at 25 °C (±2 °C);

Step 2: Let the battery rest for 3 min and record the voltage curve changes;

Step 3: Extract HFs and input them into a model trained using a dataset without outliers to estimate SOH.

Parameters such as voltage and internal resistance are influenced by SOC, necessitating HF extraction based on fixed SOC. Since retired batteries are tested offline, they can be discharged at a constant current. However, they cannot be directly discharged to a specific SOC with an unknown SOH. To solve the problem, this paper proposes discharging the battery to the specified voltage and analyzing the resting voltage to extract HFs. Initially, we discharged the retired battery at a constant current to the same voltage limit, ensuring consistent baselines across different retired batteries. Subsequently, in this study, we analyzed the voltage curve during a 3 min resting period.

The analysis of the proposed method is explained as follows: Common equivalent circuit models include the Rint model, Randles model, PNGV model, n-order RC model, and RC fractional-order model. These models exhibit varying trade-offs between accuracy and computational complexity. Figure 1 illustrates the Thevenin equivalent circuit model, known for its simplicity and high accuracy. It comprises OCV, Ohmic resistance (R_0), polarization resistance (R_1), and capacitance. R_0 encompasses contact and wire resistances. The terminal voltage of the battery consists of three components: the OCV, the voltage component attributed to R_0, and the voltage component shared by R_1 and C. R_0 refers to the resistance within the battery, comprising the resistance of electrode materials, the electrolyte, and the separator, as well as the contact resistance between various components. R_1 refers to the additional resistance generated during the charging and discharging process of the battery due to the electrode reactions. C is used to simulate the charge storage and release behavior of the battery during charging and discharging. Both R_0 and R_1 are influenced by the current. In Figure 1, when the battery charges, the current I is positive. The current is negative when discharging.

$$U_{\mathrm{ct}} = R_0 I + I R_1 \mathrm{e}^{(-C_1 R_1 t)} + U_{\mathrm{ocv}} \tag{2}$$

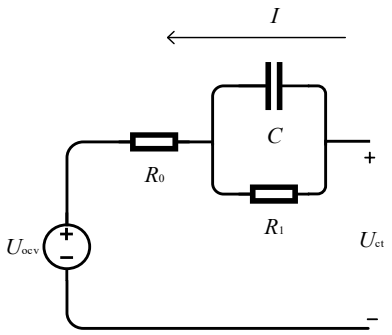

Figure 1. Thevenin equivalent circuit model.

As batteries age, the concentration of active materials and electrolytes within the battery gradually decreases while the thickness of solid-state electrolyte membranes increases. Consequently, the resistance encountered by electrons and ions during their movement within the battery increases, leading to a gradual rise in internal resistance. As depicted in Figure 1, the terminal voltage of a battery is determined by the OCV, internal resistance, and current. When all retired batteries are tested with the same discharge current and at the same cutoff voltage, the retired battery with higher internal resistance will correspond to a higher OCV at discharge termination. As the discharge process halts, the voltage components attributed to R_0 and R_1 rapidly drop, and the battery terminal voltage gradually stabilizes. Therefore, when discharge ceases, the retired battery with greater aging exhibits a higher remaining SOC and, correspondingly, a higher OCV. This characteristic motivates our approach of extracting HFs from the voltage variation after discharge cessation. However, the choice of the discharge voltage lower limit impacts the differences in resting voltages among batteries with varying SOHs.

As shown in Figure 2, the OCV of lithium iron phosphate batteries exhibits minimal variation within the SOC range from 10% to 90%. However, near an SOC of 0% or 100%, the OCV changes greatly. When the battery SOC approaches 0%, even small SOC differences are discernible in the battery voltage. This property allows us to extract HFs from the battery voltage, particularly when the SOC is low. Based on this analysis, we discharged retired batteries at a constant current to a consistent lower voltage limit and subsequently extracted HFs from the voltage curves. Choosing an appropriate discharge voltage lower limit facilitates the differentiation of SOCs among different retired batteries based on their voltage responses. However, the selection of this voltage limit remains an analytical consideration. If the chosen value for the discharge voltage lower limit is too high, the remaining SOCs of retired batteries may fall between 10% and 90%. In such cases, due to the flat region in the lithium iron phosphate battery voltage curve (as seen in Figure 2), it becomes challenging to analyze SOC differences among batteries with varying SOHs.

If the discharge voltage lower limit is set too low, the SOC differences among different SOH batteries become minimal, resulting in correspondingly small voltage differences. Typically, for lithium iron phosphate batteries, the discharge voltage lower limit is set between 2 V and 2.5 V to avoid over-discharging, which could cause permanent damage to the battery. If accurate capacity estimation of retired batteries is required, the discharge cutoff voltage should be set as low as possible within a safe range to ensure that high internal resistance batteries are adequately discharged. Conversely, if the goal is to observe voltage differences among different SOH batteries after discharge cessation, the discharge voltage lower limit should not be too low, allowing low SOH batteries to discharge fully while preventing excessive discharge for high SOH batteries. Therefore, in this study, we selected a discharge voltage lower limit of 2.5 V. At this level, the SOC of batteries with high internal resistance and low SOH approaches 0, while the SOC of batteries with low internal resistance and high SOH remains above 0. After discharge stops, the battery terminal

voltage rapidly rebounds, and the rate and magnitude of voltage recovery differ among batteries with varying SOHs.

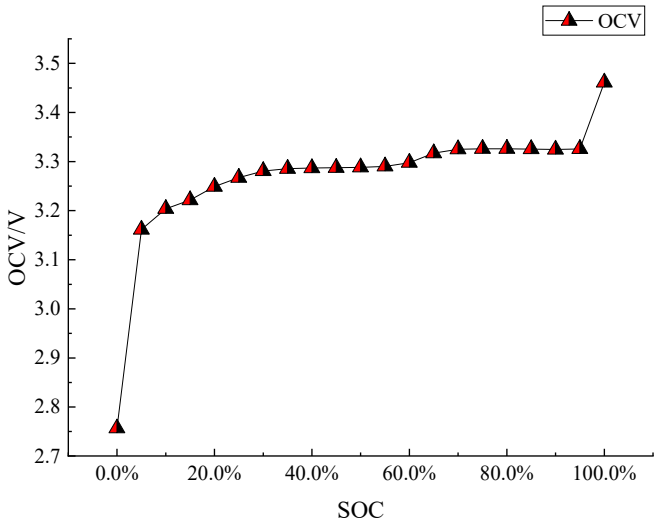

Figure 2. Open-circuit voltage versus SOC at 25 °C.

OCV measurements typically require several hours of resting time for retired batteries, resulting in a time-consuming process of SOH estimation. Therefore, we analyzed voltage changes during a 3 min resting period after the end of discharging. The retired batteries selected in Figure 3 were sourced from five electric vehicles with different historical experiences. As shown in Figure 3, different SOH retired batteries were discharged to the same voltage of 2.5 V.

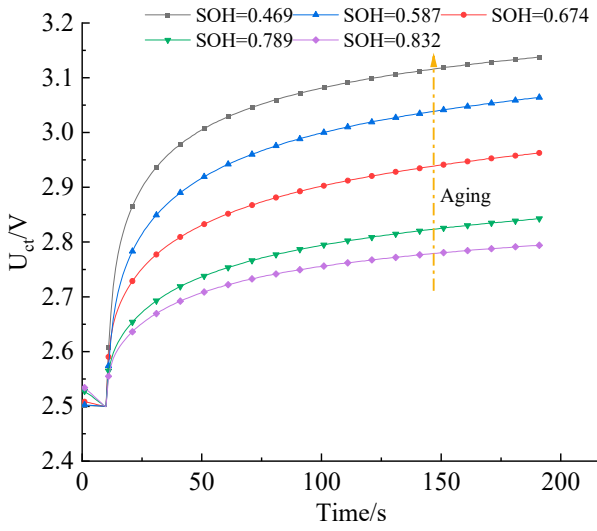

Figure 3. Variation of resting voltage with time for different SOH cells.

When discharge stops, the battery voltage rapidly rebounds. After approximately 20 s of resting, the rate of voltage recovery gradually slows down, eventually stabilizing. As depicted in Figure 3, with increasing SOH, the voltage increment during the resting process diminishes. This phenomenon occurs because high SOH batteries discharge fully, resulting in lower remaining SOC when the discharge voltage reaches 2.5 V. Conversely, low SOH batteries, due to increased internal resistance, exhibit higher remaining SOC. Leveraging this characteristic, our approach extracts HFs to achieve rapid SOH estimation for retired batteries.

As shown in Figure 4, to fully utilize the battery voltage during the resting process, it is essential to divide this period into equidistant intervals. If the chosen interval is too large, the resting process may not be fully exploited. In this study, the resting voltage recovery

process is divided into six intervals and select specific time points after discharge cessation (V_1, V_2, V_3, V_4, V_5, and V_6) as HFs. These time points correspond to the battery voltage at 30 s, 60 s, 90 s, 120 s, 150 s, and 180 s after the start of the resting phase. These voltages are used to analyze the magnitude of voltage recovery after constant current discharge. As the SOH of a battery increases, the remaining SOC at the end of constant current discharge also rises, resulting in higher voltage recovery. Therefore, V_1, V_2, V_3, V_4, V_5, and V_6 exhibit a negative correlation with SOH, which justifies their selection as HFs. The following sections will elaborate on the principles of HF extraction strategy and the rationale behind selecting six specific HFs.

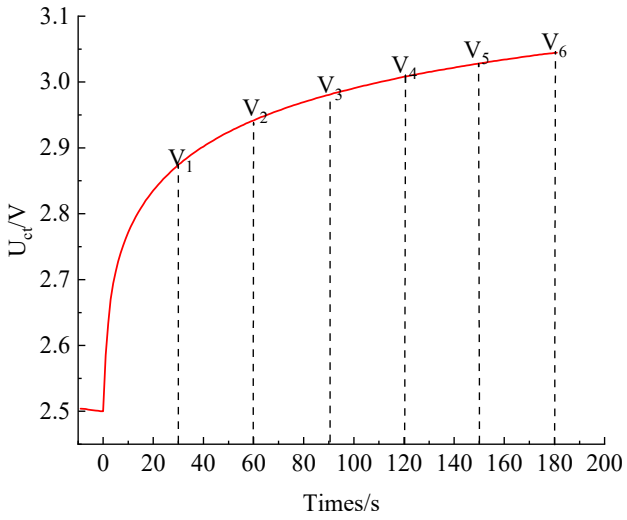

Figure 4. Schematic diagram of characteristic voltage selection at 25 °C.

3. The Strategy for Fast SOH Estimation

Since the SOH assessment of retired batteries occurs in an offline context, data-driven algorithms can rely on computationally powerful computers for SOH estimation. Both HFs and data-driven algorithms significantly influence SOH estimation, as discussed in the previous section. This paper elaborated on the rationale behind selecting HFs. Based on the analysis presented earlier, this paper proposes the following specific steps for HF acquisition:

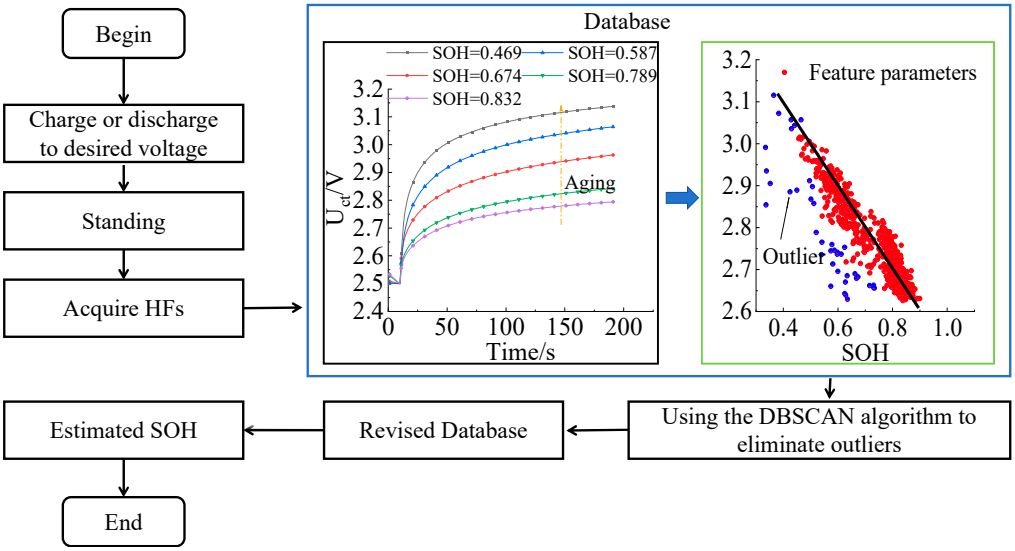

Figure 5. The flow of fast SOH estimation.

As shown in Figure 5, discharge the retired batteries to a predetermined lower voltage limit of 2.5 V. For batteries with OCV below 3.2 V, a preliminary 10% rated capacity charge is necessary before discharging to the 2.5 V voltage limit.

Allow the retired batteries to rest for 3 min and record the voltage curve during this period.

Given that the SOCs of retired batteries with varying SOHs differ at this point, the voltage recovery amplitude after discharge cessation will also vary. Extract HFs (V_1, V_2, V_3, V_4, V_5, and V_6) from the resting voltage curve. After selecting appropriate HFs, the next section will discuss how to effectively utilize SOH features to achieve rapid SOH estimation for retired batteries. This paper will explore two aspects: selecting regression algorithms for retired batteries and addressing the impact of outliers in test data on SOH estimation accuracy.

3.1. Support Vector Regression

To fully utilize the HFs from the resting voltage curve, this study employs the SVR algorithm in conjunction with HFs to construct an SOH estimation model. SVR is a regression method based on support vector machines, which organizes all sample points onto a hyperplane, aiming to minimize the distance of the smallest sample point from the hyperplane. By introducing the penalty parameter C and the slack variable ε controlling the insensitive loss function, the optimal regression hyperplane is determined. For regression problems, the optimal hyperplane should satisfy

$$\begin{aligned} &\min_{\omega,b} \tfrac{1}{2} \parallel \omega \parallel^2 + C\sum^{n}(\xi_i + \xi_i^*) \\ &\text{s.t.} \begin{cases} y_i - \omega x_i - b \le \epsilon + \xi_i \\ \omega x_i + b - y_i \le \epsilon + \xi_i^* \end{cases}, i = 1, 2, \cdots, n \end{aligned} \tag{3}$$

Constructing a Lagrangian function by introducing Lagrangian multipliers gives the following:

$$\begin{aligned} L = \tfrac{1}{2} \parallel \omega \parallel^2 + C \sum_{i=1}^{n} (\xi_i + \xi_i^*) - \sum_{i=1}^{n} \alpha_i (\epsilon + \xi_i + y_i - \omega x_i - b) \\ - \sum_{i=1}^{n} \alpha_i^* (\epsilon + \xi_i^* + y_i - \omega x_i - b) - \sum_{i=1}^{n} (\mu_i \xi_i + \mu_i^* \xi_i^*) \end{aligned} \tag{4}$$

The optimal solution is obtained by using the KKT (Karush–Kuhn–Tucker) condition, and the dyadic problem of SVR can be obtained by substituting into the Lagrangian function as follows:

$$\begin{aligned} &\max -\tfrac{1}{2} \sum_{i,j=1}^{n} (\alpha_i - \alpha_i^*) \left(\alpha_j - \alpha_j^*\right) K(x, x_i) + \\ &\sum_{i=1}^{n} y_i (\alpha_i - \alpha_i^*) - \varepsilon \sum_{i=1}^{n} (\alpha_i + \alpha_i^*) \\ &\text{s.t.} \sum_{i=1}^{n} (\alpha_i - \alpha_i^*) = 0; 0 \le \alpha_i, \alpha_i^* \le C \end{aligned} \tag{5}$$

In Equation (5), α_i, α_i^*, α_j^*, and α_j represent the Lagrange multipliers. Substituting into the regression function, the final SVR regression model is obtained as follows:

$$f(x) = \sum_{i=1}^{n} (\alpha_i - \alpha_i^*) K(x, x_i) + b \tag{6}$$

3.2. Density-Based Spatial Clustering of Applications with Noise

In the testing of retired batteries, some batteries may produce outlier data due to measurement reasons. Outliers typically refer to data points with significantly large residuals where the predicted y-values deviate significantly from the true y-values. If outliers are not correctly detected and handled, the training set containing outliers cannot effectively train a regression algorithm model. Incorrect data or outlier data that deviate from normal

test values should be corrected or removed. Outliers can impact the accuracy of regression prediction models for retired battery testing. To address this, this paper proposes using the DBSCAN (Density-Based Spatial Clustering of Applications with Noise) algorithm to identify outlier data points within the retired battery test dataset.

The DBSCAN clustering algorithm relies on the distance between object points and core points and is a density-based clustering method. It defines a cluster as a group of sufficiently dense connected points and can discover clusters of any shape. Outlier data points in test datasets generally exist as individual points or clusters, with individual points or clusters deviating significantly from the majority of data. Outliers can affect the regression coefficients in the regression model, thus impacting the training accuracy of the regression model. The advantages of the DBSCAN algorithm include not requiring prior knowledge of the number of clusters, the ability to discover clusters of any shape, and the ability to identify and handle noise points. This paper proposes using the DBSCAN clustering algorithm to identify outlier points in the battery training set and subsequently remove these outlier points from the training set. The working principle of the DBSCAN algorithm is as follows:

For each point in the retired battery training set, if the number of sample points within its neighborhood (centered around the point with a radius of epsilon) is greater than or equal to MinPts, create a new cluster. Extend this cluster by adding all directly density-reachable points within their neighborhoods.

Then, check the neighborhoods of these points in the same manner. If the number of sample points within the neighborhood is greater than or equal to MinPts, continue adding them to the cluster. This process continues until the cluster no longer expands.

If there are still unvisited points, repeat steps 1 and 2 for each new unvisited point until all points have been visited.

Battery operation conditions typically vary within a certain range, resulting in relatively stable degradation trajectories for battery performance parameters. However, during retired battery testing, inevitable measurement errors can cause some battery voltages and currents to deviate from normal values. Additionally, features of faulty batteries may also deviate from the normal range. The DBSCAN algorithm can identify outlier battery points in the training set, ensuring that outlier points do not adversely affect the accurate modeling of the SVR model. The proposed strategy for rapid SOH estimation of retired batteries in this study follows these steps:

Training Set Acquisition: Randomly select a certain number of retired batteries and use the ampere-hour integration method to obtain accurate SOH by fully charging and discharging the retired batteries twice. Subsequently, discharge these batteries to the 2.5 V discharge voltage lower limit, allow them to rest for 3 min, and record the corresponding voltages to extract HFs.

Identify Outliers Using DBSCAN: Apply the DBSCAN clustering algorithm to identify outlier HFs and corresponding abnormal data points in the training set. Remove these outlier points from the training set. Train the SVR model using the filtered HFs and SOH.

SOH Estimation for Unknown Retired Batteries: If the OCV is less than 3.1 V, charge the retired battery to 10% of the rated capacity and allow it to rest for 10 min. Then, discharge the battery to the 2.5 V discharge voltage lower limit and rest for 3 min to extract HFs. Input the HFs into the trained SVR model to obtain the corresponding SOH. If the OCV is greater than 3.1 V, discharge the retired battery to the 2.5 V discharge voltage lower limit and rest for 3 min to extract HFs. Input the HFs into the trained SVR model to obtain the corresponding SOH. The methodology presented in this paper is generally applicable to other types of chemical batteries. However, the lower limit of discharge voltage needs to

be re-selected, and the SOH estimation model needs to be constructed using a dataset of characteristics specific to the other types of chemical batteries.

4. Experiment and Discussion

To validate the effectiveness of the proposed strategy for SOH estimation of retired batteries, this paper established the following testing platform. The retired lithium iron phosphate batteries selected in this paper come from electric vehicles. These batteries had a rated capacity of 30 AH at the time of manufacture, but their historical experiences are diverse and unknown. The testing platform consists of a battery test cabinet, a temperature-controlled chamber, and an upper-level computer system produced by Newway Corporation. The battery test cabinet enables accurate capacity measurement through charge and discharge cycles, the temperature-controlled chamber provides controlled testing temperatures, and the upper-level computer collects and records current and voltage data. To mitigate the impact of temperature on experimental results, the environmental testing temperature was maintained at 25 °C (±2 °C).

To verify the rationality of selecting the discharge cutoff voltage, this paper selected two retired batteries with SOH values of 0.9 and 0.67. The following steps were performed for both batteries:

(1) Charged the two retired batteries with a current of 20 A for 10 min to ensure sufficient charge.

(2) Allowed the batteries to rest for 30 min to stabilize internal reactions.

(3) Discharged the two retired batteries to 2 V using a constant current of 20 A, followed by a 3 min rest period.

Repeated steps (1) to (3) by modifying the discharge cutoff voltage to 2.1 V, 2.3 V, 2.5 V, 2.7 V, and 2.9 V until completion.

As shown in Figure 6, significant differences in voltage recovery during the resting period were observed among retired batteries with varying SOHs after being discharged to the same lower voltage limit. Lower discharge voltage limits resulted in larger voltage recovery amplitudes during resting, validating the appropriateness of the previously described discharge cutoff voltage selection.

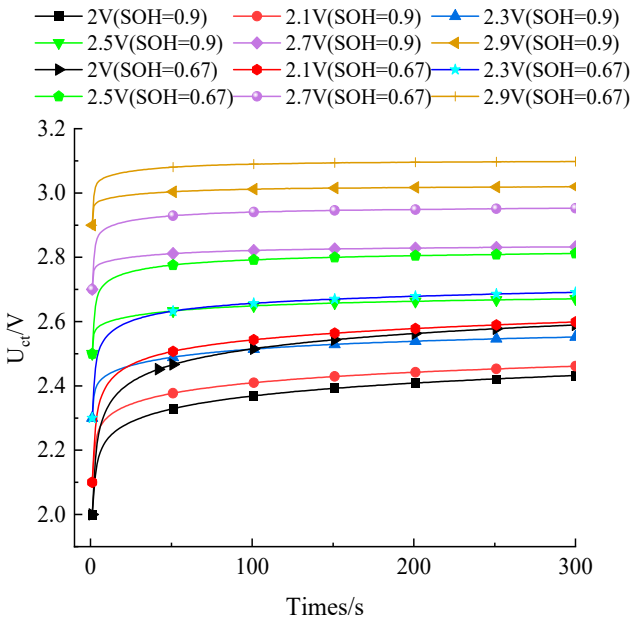

Figure 6. The resting voltage of batteries with different SOHs at various cutoff voltages.

Table 1 presents the voltage differences (V_1, V_2, V_3, V_4, V_5, and V_6) corresponding to the resting periods of 30 s, 60 s, 90 s, 120 s, 150 s, and 180 s after discharge completion. Larger voltage differences associated with different SOH batteries indicate greater variations in feature voltages due to battery aging. Feature voltages with larger variations across SOHs facilitate better discrimination among different battery states. Notably, when the discharge cutoff was set to 2.3 V or 2.5 V, the largest V_1 difference occurred between SOH = 0.67 and SOH = 0.9. Additionally, when the discharge cutoff was set to 2.3 V, the V_1 and V_2 differences between SOH = 0.67 and SOH = 0.9 were maximized. However, the V_1 and V_2 differences were similar when the discharge cutoff was set to 2.3 V or 2.5 V. Finally, when the discharge cutoff was set to 2.5 V, the largest differences in V_3, V_4, V_5, and V_6 occurred between SOH = 0.67 and SOH = 0.9. Consequently, this paper selected 2.5 V as the discharge voltage lower limit for our approach.

Table 1. Characteristic voltage difference values corresponding to SOH = 0.9 and SOH = 0.67 at different discharge voltage limits.

		2 V	2.1 V	2.3 V	2.5 V	2.7 V	2.9 V
V_1/V	**SOH = 0.9**	2.3000	2.3533	2.4708	2.6212	2.8035	2.9969
	SOH = 0.67	2.4283	2.4786	2.6112	2.7613	2.9185	3.0713
	Difference	0.1283	0.1253	0.1404	0.1401	0.1150	0.0744
V_2/V	**SOH = 0.9**	2.3397	2.3859	2.4959	2.6373	2.8140	3.0062
	SOH = 0.67	2.4795	2.5170	2.6395	2.7805	2.9324	3.0831
	Difference	0.1398	0.1311	0.1436	0.1432	0.1184	0.0769
V_3/V	**SOH = 0.9**	2.3629	2.4051	2.5108	2.6463	2.8199	3.0106
	SOH = 0.67	2.5080	2.5381	2.6534	2.7898	2.9389	3.0884
	Difference	0.1451	0.1330	0.1426	0.1435	0.1190	0.0778
V_4/V	**SOH = 0.9**	2.3794	2.4184	2.5213	2.6528	2.8236	3.0137
	SOH = 0.67	2.5282	2.5527	2.6627	2.7960	2.9433	3.0915
	Difference	0.1488	0.1343	0.1414	0.1432	0.1197	0.0778
V_5/V	**SOH = 0.9**	2.3924	2.4293	2.5291	2.6578	2.8258	3.0152
	SOH = 0.67	2.5437	2.5638	2.6698	2.7997	2.9458	3.0936
	Difference	0.1513	0.1345	0.1407	0.1419	0.1200	0.0784
V_6/V	**SOH = 0.9**	2.4026	2.4376	2.5353	2.6612	2.8276	3.0164
	SOH = 0.67	2.5558	2.5728	2.6757	2.8031	2.9476	3.0949
	Difference	0.1532	0.1352	0.1404	0.1419	0.1200	0.0785

Firstly, 830 retired lithium iron phosphate batteries with a rated capacity of 30 Ah were randomly selected and divided into training and testing sets. The training set is used to train the SVR model, while the testing set is used to validate the accuracy of the trained SVR model in estimating SOH.

To obtain the true SOH, we initially performed complete charge and discharge cycles on the retired batteries. The specific implementation strategy is as follows:

Charge the retired batteries with a constant current of 20 A until the upper voltage limit of 3.65 V is reached.

Maintain a constant voltage until the current drops to 1 A.

Discharge the retired batteries with a constant current of 20 A until the voltage decreases to the lower cutoff voltage of 2 V.

Repeat the above process twice, considering the charge released by the retired batteries during the discharge process as their capacity.

To quantitatively describe the effectiveness of SOH estimation, we calculated the root-mean-square error (RMSE) for SOH estimation as follows:

$$RMSE = \sqrt{\frac{1}{N}\sum_{i=1}^{N}(\mathrm{SOH}_{\mathrm{real}}(i)\text{-}\mathrm{SOH}_{\mathrm{estimate}}(i))^2} \quad (7)$$

In Equation (7), $\mathrm{SOH}_{\mathrm{real}}$ represents the true SOH of the battery, $\mathrm{SOH}_{\mathrm{estimate}}$ denotes the estimated battery SOH, and N represents the number of tested batteries.

Figure 7 describes the variation of HFs, including V_1, V_2, V_3, V_4, V_5, and V_6, with the SOH of 800 retired batteries in the training set. In Figure 7, as the SOH value decreases, indicating higher battery aging, the corresponding HF values also decrease. However, due to the varying historical operating conditions experienced by different retired batteries, the aging magnitude of HFs differs. Consequently, this correlation is not strictly linear. Relying solely on individual HFs for accurate SOH estimation becomes challenging. Therefore, in the next section, this paper will discuss how to leverage the SVR algorithm in combination with multiple HFs to achieve SOH estimation for retired batteries. As shown in Figure 7, HFs exhibit a negative correlation with SOH.

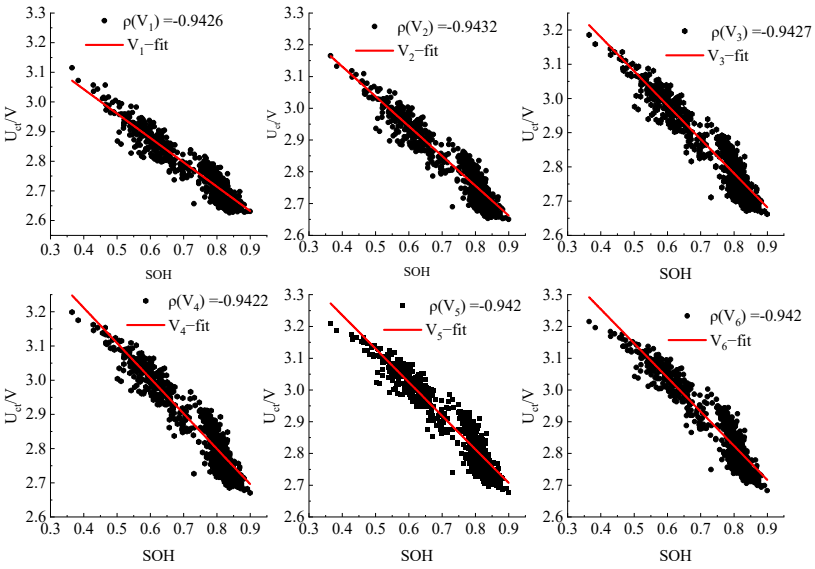

Figure 7. Variation of characteristic voltage with SOH without noise.

To analyze the correlation between the selected features and SOH, we calculated the Pearson correlation coefficient between SOH and HFs as follows:

$$\rho = \frac{\sum(f_i - \overline{f_i})(SOH - \overline{SOH})}{\sqrt{\sum(f_i - \overline{f_i})^2 (SOH - \overline{SOH})^2}} \quad (8)$$

In Equation (8), ρ represents the Pearson correlation coefficient between the HFs and the SOH, and f_i denotes the (i)-th sample in the HFs and represents the average value of the HF samples.

By combining the aforementioned features, this paper can fully utilize the SOH information contained in the voltage during the resting process, thereby improving the accuracy of SOH estimation. Figure 8 illustrates how the correlation ρ between the voltage during battery resting and SOH changes over time. As shown in Figure 8, the correlation between the resting voltage and SOH gradually increases with the duration of resting. As resting time increases, the voltage differences among retired batteries with varying SOHs become more pronounced. Within the same time frame, batteries with lower SOHs exhibit faster

and larger voltage changes, resulting in a higher correlation ρ between battery voltage and SOH after 20 s of resting. This motivates our choice of using the battery voltage after 30 s of resting as the HFs. Figure 8 depicts the trend of feature voltages during resting with respect to SOH.

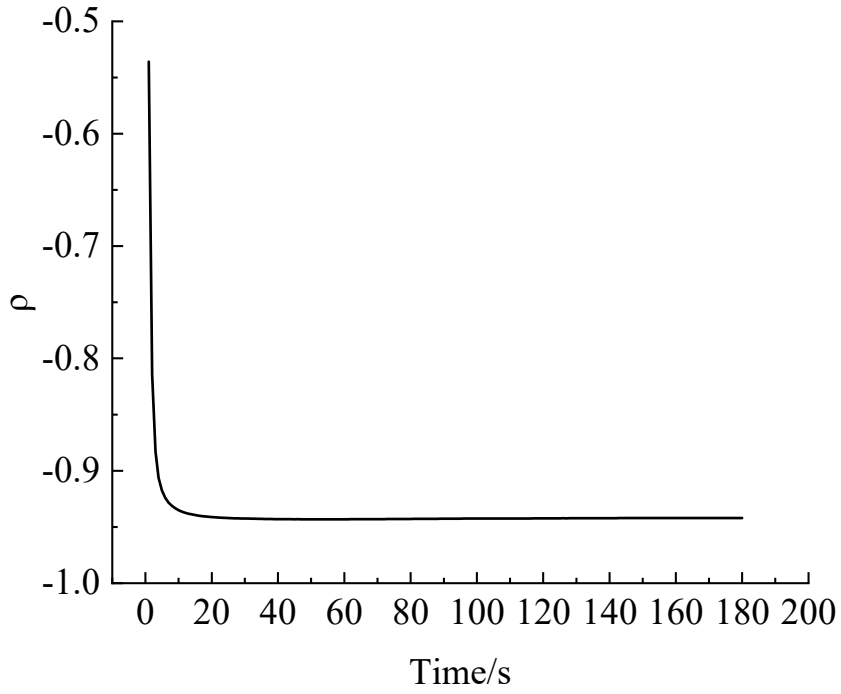

Figure 8. Correlation coefficient between resting voltage and SOH.

4.1. Data Preprocessing

In order to verify the effect of outliers in the training set on the SOH estimation and the effect of DBSCAN's clustering algorithm on the SOH estimation after identifying the outliers in the training set, we designed the following experimental procedure. Num batteries are selected from the training set, and their actual SOH is added to Gaussian noise to simulate the outliers formed due to detection errors or internal battery faults.

$$\mathrm{SOH}_{noise} = \mathrm{SOH}_{\mathrm{real}} - \eta * rand \tag{9}$$

In Equation (9), η describes the maximum deviation of battery SOH from the true SOH, where in this study, η is set to 0.25, and rand represents a random number between 0 and 1.

As shown in Figure 9, within the dataset augmented with Gaussian noise, outliers deviate from the majority of batteries in a random manner. The normal batteries are unified as red points, and the batteries polluted by noise are modified as blue points.

The proposed approach involves the following steps:

Initially, the training set includes 800 retired batteries with outlier data. An SVR model is trained using this dataset.

Next, the trained SVR model estimates the SOH for a testing set containing 30 batteries.

Subsequently, the DBSCAN clustering algorithm is applied to identify the outlier points.

Finally, the SVR algorithm is trained using the training set, excluding the identified outliers. The trained SVR model is then used to estimate the SOH for the testing set.

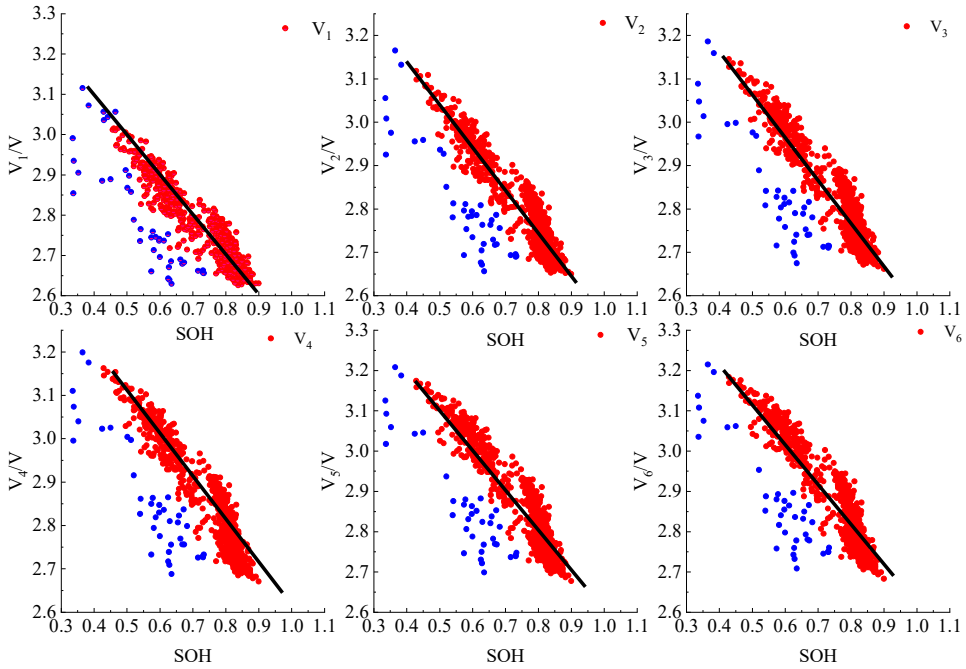

Figure 9. Variation of characteristic voltage with SOH in noise.

In Figure 9, the parameter 'Num' takes a value of 50. As depicted in Figure 9, the DBSCAN clustering algorithm defines clusters by grouping density-sufficient outlier points, even identifying individual batteries that deviate significantly from the majority. The presence of outliers can distort the SVR algorithm model, affecting the accuracy of SOH estimation. Before training the SVR model on the training set, the batteries corresponding to V_1, V_2, V_3, V_4, V_5, and V_6 are sequentially identified as outliers and removed from the training set. The largest cluster in terms of data volume serves as the training set for the SVR model, while the batteries identified as outliers are excluded from the training set to prevent their impact on SOH estimation accuracy.

4.2. The Estimation Result Validation of SOH

To validate the advantages of the proposed rapid SOH estimation approach, we selected 30 retired batteries as the testing set. In the following discussion, this paper will explore the comparison of SOH estimation times and the impact of the DBSCAN algorithm on SOH estimation accuracy. Adaptive filtering algorithms, exemplified by the Kalman filter, continuously improve SOH estimation accuracy through iterative processes. However, these methods face limitations due to the unavailability of history data for retired batteries.

Traditional SOH estimation methods include the ampere-hour integration method, EIS, and incremental capacity method. Unfortunately, applying these methods to offline scenarios for the SOH estimation of retired batteries has its drawbacks. For instance, EIS estimation is influenced by battery SOC, which remains unknown during retired battery testing. Additionally, EIS measurements require expensive equipment. The incremental capacity method involves charging and discharging batteries with low currents, followed by extracting HFs from voltage curves. This process remains time-consuming. The ampere-hour integration method remains the primary approach for the SOH estimation of retired batteries despite its slow speed. However, our proposed SOH estimation strategy offers a faster alternative.

In Figure 10, the initial SOC distribution of the testing set's retired batteries is depicted using a line graph. The SOC values for these batteries randomly span between 0 and 1. The bar charts in Figure 10 illustrate the time consumption for SOH estimation using both the ampere-hour integration method and our proposed approach under a 20 A

charge–discharge current. Notably, our method achieves shorter SOH estimation times for retired batteries with lower SOCs. When the SOC of retired batteries approaches 1, our SOH estimation strategy moderately reduces the time required for SOH assessment. For batteries with an SOC close to 0, our approach significantly shortens the SOH estimation time. Compared to traditional SOH estimation methods, our proposed approach leverages inexpensive battery test cabinets, is applicable to batteries with unknown SOCs, and provides faster testing speeds.

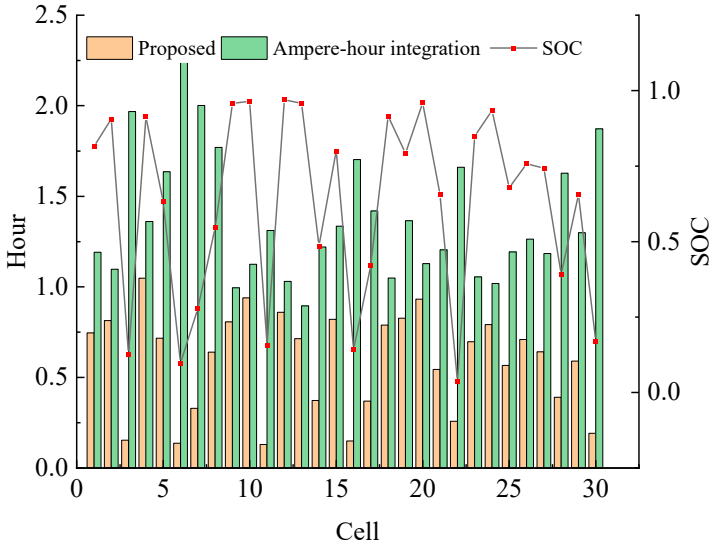

Figure 10. Comparison of estimated time for SOH.

As shown in Figure 11, when the SVR model is trained using a training set containing colored noise, the trained SVR model cannot adequately match the training set. If the inaccurate SVR model is used to estimate the SOH of decommissioned batteries using HFs, the accuracy of the SOH estimation results will not be guaranteed.

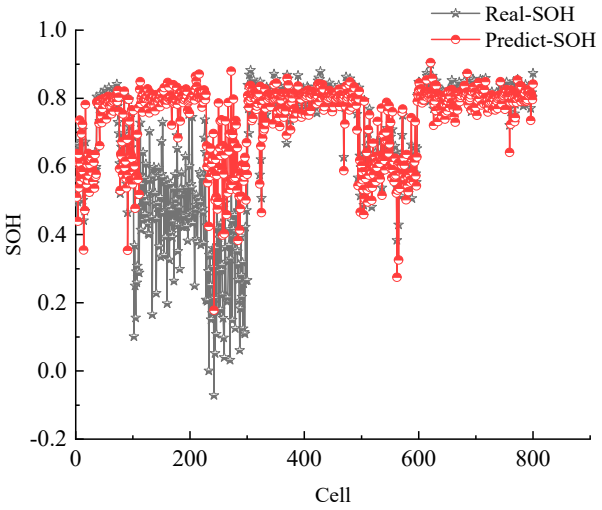

Figure 11. The deviation in predictions made by the model trained on noisy data.

As shown in Figure 12, directly training the SVR model using a training set augmented with Gaussian noise outliers (Num = 200) results in a root-mean-square error (RMSE) of 0.033 for estimating the SOH of batteries in the testing set. In comparison, the RFR algorithm yields an RMSE of 0.057, the DBSCAN-RFR hybrid approach achieves an RMSE of 0.038, and the DBSCAN-SVR method, proposed in this study, achieves an RMSE of 0.028. From Figure 12, it is evident that the DBSCAN-SVR approach provides SOH estimates that

closely align with the majority of battery SOH values, validating the effectiveness of using the DBSCAN algorithm to identify outlier points and enhance retired battery SOH estimation.

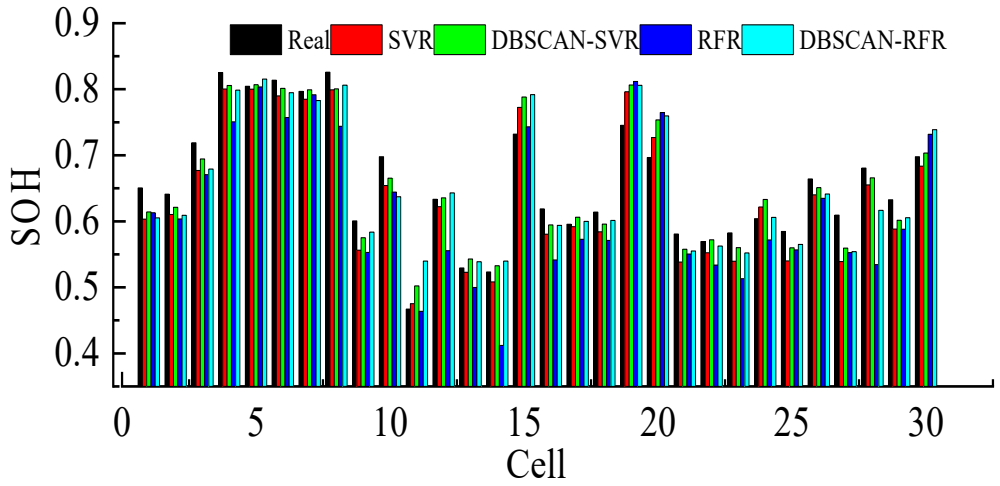

Figure 12. Comparison of SOH estimation results with Gaussian noise outliers.

In practical measurements, the error, in addition to Gaussian noise, will also exist in colored noise and zero drift. In order to verify the effect of the DBSCAN algorithm in identifying the outliers containing colored noise in the training set, the following experiments were carried out:

The colored noise model selected in this paper is as follows:

$$\mathrm{noise}_{k+1} = \lambda_{k+1,k}\mathrm{noise}_k + \zeta_k \tag{10}$$

$$\mathrm{SOH}_{color-noise} = \mathrm{SOH}_{real} + \mathrm{noise}_{color} - c \tag{11}$$

where noise_k is the colored noise, $\lambda_{k+1,k}$ is the colored noise transfer matrix, ζ_k is the zero-mean white noise, and c is the fixed bias when simulating measurements with fixed values.

Directly using the training set containing colored noise outliers (Num = 200) to train the SVR model to estimate the SOH of the battery in the test set has a root-mean-square error of 0.032, the RFR algorithm estimates SOH with a root-mean-square error of 0.0769, the DBSCAN-RFR algorithm estimates SOH with a root-mean-square error of 0.0335, and the DBSCAN-SVR method is used to estimate battery SOH with a root-mean-square error of 0.0289. As shown in Figure 13, similar to training the regression algorithm model with a training set containing Gaussian noise, the DBSCAN algorithm is able to significantly improve the SOH estimation accuracy of the RFR algorithm. SVR aims to find a hyperplane that minimizes prediction error and establishes a margin around this hyperplane, within which the majority of samples reside. On the other hand, RFR is an ensemble learning method that constructs a set of models based on decision trees. It trains a sub-model on each decision tree by performing bootstrap sampling on the dataset and randomly selecting features, then obtains the final prediction by averaging or weighting the predictions of all sub-models. In the example presented in this paper, only a portion of the batteries were subjected to noise, and the predictions made by SVR consistently relied on the majority of the battery training set, resulting in relatively stable predictions. However, in this study, all six selected features were subjected to noise, and the training sets for RFR's random feature selection were contaminated, leading to unstable and inaccurate predictions by RFR.

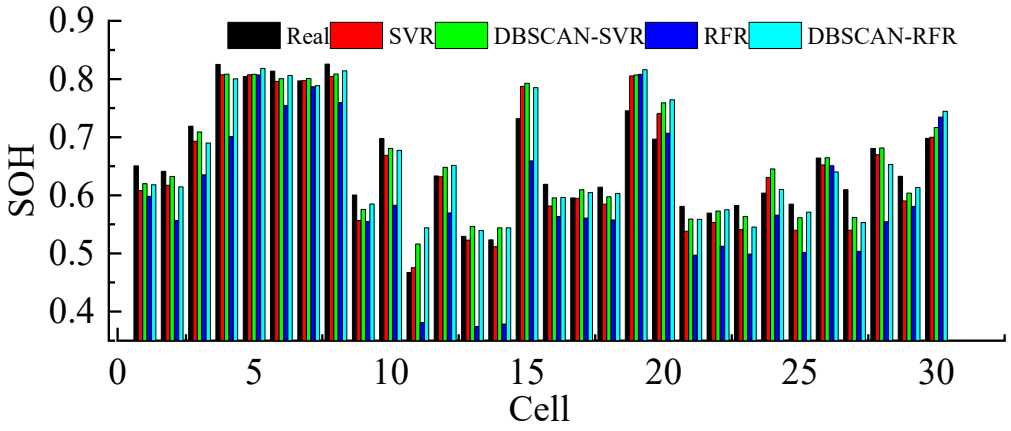

Figure 13. Comparison of SOH estimation results without Gaussian noise outliers.

Although the effect of the SVR model used in this paper to estimate SOH is relatively less affected by outliers, the DBSCAN algorithm still reduces the effect of outliers on the SVR model.

The RMSE values of the SVR and DBSCAN-SVR models for estimating the SOH error of the training set are depicted in Figure 13 for the SVR and DBSCAN-SVR models, respectively, when there are different numbers of outlier points in the training set. Num in Figure 13 indicates the number of outlier points in the training set, and DBSCAN-Num indicates that the outlier points in the training set have been identified by the DBSCAN algorithm. As shown in Figure 13, when the number of outlier points in the training set increases, the RMSE value of SOH estimation error keeps increasing, which indicates that the number of outlier points in the sample affects the accuracy of battery modeling. Meanwhile, it can be seen from Figure 13 that as the number of outlier points in the sample increases, the greater the magnitude of the reduction of SOH estimation error after the DBSCAN algorithm proposed in this paper identifies the outlier points.

5. Conclusions

This paper proposes a method for fast SOH estimation based on the voltage and resistance of the battery to pulse current. Firstly, the reasons for selecting HFs proposed in this paper from the resting voltage curves and the process of obtaining them are proposed in this paper. Then, the rapid SOH estimation strategy and how to use the DBSCAN algorithm to filter out outliers in the training datasets are described. Eventually, the effectiveness of the proposed method is verified by describing the reasons for selecting a discharge voltage of 2.5 V, the impact of outliers on SOH estimation, the improvement in SOH estimation accuracy after removing outliers using the DBSCAN algorithm, and the reduction in SOH estimation time. This algorithm can quickly estimate the battery's approximate SOH compared to traditional methods. Simultaneously, the SOC-related characteristic parameters chosen in this paper can be used as a guide for quickly sorting retired batteries. But, there is still room to improve the accuracy of SOH estimation. There are differences in the performance of different types of batteries, so the correlation between SOH and the HFs of different types of batteries is different. Based on the findings of this paper, future research will focus on how to use analysis and comparison of retired battery parameters under the same SOC or how to charge the battery to the desired SOC to achieve sorting of retired batteries.

Author Contributions: Conceptualization, X.L.; methodology, X.L.; software, Y.W.; validation, Y.W.; formal analysis, Y.W.; investigation, W.C.; resources, W.C.; data curation, X.L.; writing—original draft preparation, X.L.; writing—review and editing, H.H.; visualization, Y.W.; supervision, H.H.; project administration, H.H.; funding acquisition, H.H. All authors have read and agreed to the published version of the manuscript.

Funding: This research was funded by the Major Science and Technology Project of Anhui Province, grant number 18030901064.

Data Availability Statement: The raw data supporting the conclusions of this article will be made available by the authors on request.

Conflicts of Interest: Author Wenjing Chang is employed by the State Grid Anhui Ultra High Voltage Company. The remaining authors declare that the research was conducted in the absence of any commercial or financial relationships that could be construed as a potential conflict of interest.

References

1. Yang, S.; Zhang, C.; Jiang, J.; Zhang, W.; Zhang, L.; Wang, Y. Review on state-of-health of lithium-ion batteries: Characterizations, estimations and applications. *J. Clean. Prod.* **2021**, *314*, 128015. [CrossRef]
2. Zhang, X.; Han, Y.; Zhang, W. A Review of Factors Affecting the Lifespan of Lithium-ion Battery and its Health Estimation Methods. *Trans. Electr. Electron. Mater.* **2021**, *22*, 567–574. [CrossRef]
3. Luo, K.; Chen, X.; Zheng, H.; Shi, Z. A review of deep learning approach to predicting the state of health and state of charge of lithium-ion batteries. *J. Energy Chem.* **2022**, *74*, 159–173. [CrossRef]
4. Lai, X.; Deng, C.; Tang, X.; Gao, F.; Han, X.; Zheng, Y. Soft clustering of retired lithium-ion batteries for the secondary utilization using Gaussian mixture model based on electrochemical impedance spectroscopy. *J. Clean. Prod.* **2022**, *339*, 130786. [CrossRef]
5. Luo, F.; Huang, H.; Ni, L.; Li, T. Rapid prediction of the state of health of retired power batteries based on electrochemical impedance spectroscopy. *J. Energy Storage* **2021**, *41*, 102866. [CrossRef]
6. Fu, Y.; Xu, J.; Shi, M.; Mei, X. A Fast Impedance Calculation-Based Battery State-of-Health Estimation Method. *IEEE Trans. Ind. Electron.* **2022**, *69*, 7019–7028. [CrossRef]
7. Feng, L.; Jiang, L.; Liu, J.; Wang, Z.; Wei, Z.; Wang, Q. Dynamic overcharge investigations of lithium ion batteries with different state of health. *J. Power Sources* **2021**, *507*, 230262. [CrossRef]
8. Gu, X.; See, K.; Li, P.; Shan, K.; Wang, Y.; Zhao, L.; Lim, K.C.; Zhang, N. A novel state-of-health estimation for the lithium-ion battery using a convolutional neural network and transformer model. *Energy* **2023**, *262*, 125501. [CrossRef]
9. Shi, M.; Xu, J.; Lin, C.; Mei, X. A fast state-of-health estimation method using single linear feature for lithium-ion batteries. *Energy* **2022**, *256*, 124652. [CrossRef]
10. Wang, C.; Wang, S.; Zhou, J.; Qiao, J.; Yang, X.; Xie, Y. A novel back propagation neural network-dual extended Kalman filter method for state-of-charge and state-of-health co-estimation of lithium-ion batteries based on limited memory least square algorithm. *J. Energy Storage* **2023**, *59*, 106563. [CrossRef]
11. Ma, L.; Xu, Y.; Zhang, H.; Yang, F.; Wang, X.; Li, C. Co-estimation of state of charge and state of health for lithium-ion batteries based on fractional-order model with multi-innovations unscented Kalman filter method. *J. Energy Storage* **2022**, *52*, 104904. [CrossRef]
12. Qiao, J.; Wang, S.; Yu, C.; Yang, X.; Fernandez, C. A chaotic firefly—Particle filtering method of dynamic migration modeling for the state-of-charge and state-of-health co-estimation of a lithium-ion battery performance. *Energy* **2023**, *263*, 126164. [CrossRef]
13. Li, R.; Hong, J.; Zhang, H.; Chen, X. Data-driven battery state of health estimation based on interval capacity for real-world electric vehicles. *Energy* **2022**, *257*, 124771. [CrossRef]
14. Luo, Y.-F.; Lu, K.-Y. An online state of health estimation technique for lithium-ion battery using artificial neural network and linear interpolation. *J. Energy Storage* **2022**, *52*, 105062. [CrossRef]
15. Ang, E.Y.M.; Paw, Y.C. Efficient linear predictive model with short term features for lithium-ion batteries state of health estimation. *J. Energy Storage* **2021**, *44*, 103409. [CrossRef]
16. Driscoll, L.; de la Torre, S.; Gomez-Ruiz, J.A. Feature-based lithium-ion battery state of health estimation with artificial neural networks. *J. Energy Storage* **2022**, *50*, 104584. [CrossRef]
17. Gong, Y.; Zhang, X.; Gao, D.; Li, H.; Yan, L.; Peng, J.; Huang, Z. State-of-health estimation of lithium-ion batteries based on improved long short-term memory algorithm. *J. Energy Storage* **2022**, *53*, 105046. [CrossRef]
18. Li, Q.; Li, D.; Zhao, K.; Wang, L.; Wang, K. State of health estimation of lithium-ion battery based on improved ant lion optimization and support vector regression. *J. Energy Storage* **2022**, *50*, 104215. [CrossRef]
19. Chen, Z.; Zhao, H.; Zhang, Y.; Shen, S.; Shen, J.; Liu, Y. State of health estimation for lithium-ion batteries based on temperature prediction and gated recurrent unit neural network. *J. Power Sources* **2022**, *521*, 230892. [CrossRef]

20. Su, X.; Sun, B.; Wang, J.; Zhang, W.; Ma, S.; He, X.; Ruan, H. Fast capacity estimation for lithium-ion battery based on online identification of low-frequency electrochemical impedance spectroscopy and Gaussian process regression. *Appl. Energy* **2022**, *322*, 119516. [CrossRef]
21. Zhang, Y.; Liu, Y.; Wang, J.; Zhang, T. State-of-health estimation for lithium-ion batteries by combining model-based incremental capacity analysis with support vector regression. *Energy* **2022**, *239*, 121986. [CrossRef]
22. Chen, X.Y.; Ge, M.M.; Yao, Z.T.; Zhou, Y.C. Research on Lidar filtering algorithm for rainy and snowy weather. *Chin. J. Sci. Instrum.* **2023**, *44*, 172–181.
23. Zhang, Z.P.; Li, S.; Liu, W.X.; Liu, S.X. Outlier detection algorithm based on fast density peak clustering outlier factor. *J. Commun.* **2022**, *43*, 10. [CrossRef]
24. Galeotti, M.; Cinà, L.; Giammanco, C.; Cordiner, S.; Di Carlo, A. Performance analysis and SOH (state of health) evaluation of lithium polymer batteries through electrochemical impedance spectroscopy. *Energy* **2015**, *89*, 678–686. [CrossRef]
25. Wang, L.; Qiao, S.; Lu, D.; Zhang, Y.; Pan, C.; He, Z.; Zhao, X.; Wang, R. State of health estimation of lithium-ion battery in wide temperature range via temperature-aging coupling mechanism analysis. *J. Energy Storage* **2022**, *47*, 103618. [CrossRef]
26. Mc Carthy, K.; Gullapalli, H.; Ryan, K.M.; Kennedy, T. Electrochemical impedance correlation analysis for the estimation of Li-ion battery state of charge, state of health and internal temperature. *J. Energy Storage* **2022**, *50*, 104608. [CrossRef]
27. Zhou, R.; Zhu, R.; Huang, C.-G.; Peng, W. State of health estimation for fast-charging lithium-ion battery based on incremental capacity analysis. *J. Energy Storage* **2022**, *51*, 104560. [CrossRef]
28. Zhu, J.; Wang, Y.; Huang, Y.; Gopaluni, R.B.; Cao, Y.; Heere, M.; Mühlbauer, M.J.; Mereacre, L.; Dai, H.; Liu, X.; et al. Data-driven capacity estimation of commercial lithium-ion batteries from voltage relaxation. *Nat. Commun.* **2022**, *13*, 2261. [CrossRef]
29. Yang, F.; Wang, D.; Zhao, Y.; Tsui, K.-L.; Bae, S.J. A study of the relationship between coulombic efficiency and capacity degradation of commercial lithium-ion batteries. *Energy* **2018**, *145*, 486–495. [CrossRef]
30. Guo, Y.F.; Huang, K.; Li, Z.G. Fast state of health prediction of lithium-ion battery based on terminal voltage drop during rest for short time. *Trans. China Electrotech. Soc.* **2019**, *34*, 3968–3978.
31. Tong, S.; Klein, M.P.; Park, J.W. On-line optimization of battery open circuit voltage for improved state-of-charge and state-of-health estimation. *J. Power Sources* **2015**, *293*, 416–428. [CrossRef]
32. Farmann, A.; Sauer, D.U. A study on the dependency of the open-circuit voltage on temperature and actual aging state of lithium-ion batteries. *J. Power Sources* **2017**, *347*, 1–13. [CrossRef]